ELSEVIER

Surface and Coatings Technology 149 (2002) 161–170

SURFACE & COATINGS TECHNOLOGY

www.elsevier.com/locate/surfcoat

Enhancement of aluminum oxide physical vapor deposition with a secondary plasma☆

Ning Li*, J.P. Allain, D.N. Ruzic

Department of Nuclear, Plasma and Radiological Engineering, University of Illinois, Urbana-Champaign, Urbana, IL 61801, USA

Received 15 March 2001; accepted in revised form 26 July 2001

Abstract

Reactive sputtering of aluminum oxide in a planar magnetron system is conducted with a mixture of O_2 and Ar reacting with and bombarding an aluminum target. The aluminum target is powered by a pulsed directed current (DC) bias which functions to discharge the accumulated ions on the insulating AlO_x film surface during the positive duty cycle and suppresses arc formation. A seven-turn helical antenna sits below the magnetron sputtering system in the vacuum system and delivers radio-frequency (RF) power to generate a secondary plasma in the chamber. This plasma can efficiently ionize the sputtered flux, achieving ionized physical vapor deposition (IPVD). A gridded energy analyzer (GEA) and a quartz crystal microbalance (QCM) are located in the substrate plane to allow the ion and neutral deposition rates to be determined. Electron temperature and electron density are measured by a RF compensated Langmuir probe. A RF power of 500 W significantly increases the deposition rate of AlO_x up to half of the Al deposition rate in metallic mode at the total pressure of 1.33 Pa (10 mtorr). At 3.33 Pa (25 mtorr), the ionization fraction of Al atoms reaches 90%. In addition the RF power extends the range of O_2 partial pressure in which the sputtering occurs in the metallic mode. SEM photos show that the secondary RF plasma makes the films smoother and denser due to a moderate level of ion bombardment. The deposition rates and ionization fractions fluctuate as a function of O_2 partial pressure. These variations can be explained by the combined variation of sputtering at the target, electron temperature and electron density.

Keywords: Physical vapor deposition; Ion bombardment; Radio-frequency; Reactive sputtering; Aluminium oxide

1. Introduction

Reactive sputtering is currently preferred to depositing dielectrics such as oxides and nitrides, as well as carbides and silicides, among which aluminum oxide is of particular interest because of its wide applications in material coating technologies for the protection of metallic components operating in hostile corrosive or oxidative environments [1]. In addition, aluminum oxide films show promise as possible substitutes of SiO_2 films in microelectronic devices [2]. Such applications are possible due to aluminum oxide's low refractive index, high resistivity, high mechanical hardness, high wear resistance, and high dielectric constant [1,3–7].

The implementation of reactive sputtering in DC magnetron systems has been frequently reported for deposition of highly insulating materials [4,5,8,9]. Several problems exist in using reactive DC magnetron sputtering for deposition of insulating films. One, in the process of reactive sputtering, the reactive gas forms a thin insulating film on the metal target surface, leading to charge build-up from highly-energetic incident ions. Breakdown of this charged layer occurs in the form of arcs leading to the ejection of material from the target which compromises the growing film quality. A second

☆Paper presented at 28th International Conference on Metallurgical Coatings and Thin Films, 30 April–4 May 2001, San Diego, CA, USA.

* Corresponding author. 214 NEL, 103 S. Goodwin Ave., Urbana, IL 61801, USA. Tel.: +1-217-333-6291; fax: +1-217-333-2906.

E-mail addresses: ningli@uiuc.edu (N. Li), druzic@uiuc.edu (D.N. Ruzic).

0257-8972/01/$ - see front matter
PII: S0257-8972(01)01446-3

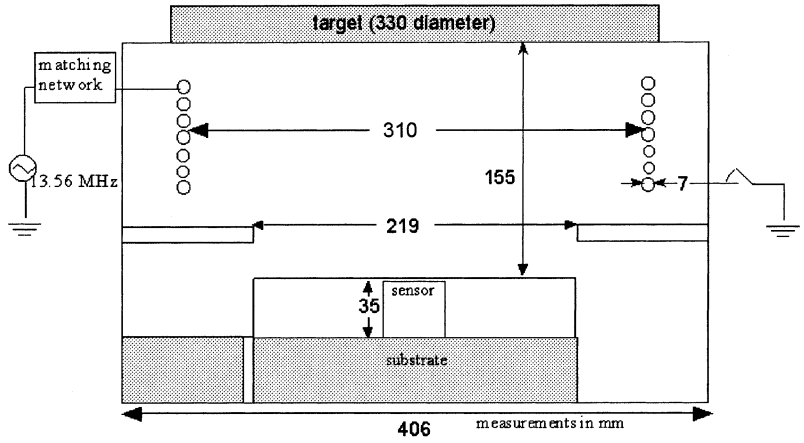

Fig. 1. Schematic of the magnetron system. A seven-turn coil sitting inside a commercial size magnetron delivers a secondary ICP. Sputtered Al atoms are partially ionized by the ICP and deposit on the substrate. The sensor simulates the position of a wafer to measure the deposition rate and ionization fraction.

problem is an enhanced reduction in the metal deposition rate due to a variety of reasons, including preferential sputtering of the oxide species formed on the metal target surface, negative ions resputtering to the substrate film, and cluster sputtering [10]. A third problem is the higher secondary electron coefficient of the insulating films formed on the target [10]. The large secondary electron emission contributes to the increase of the discharge current, which in turn decreases the target voltage in order to maintain a fixed input power. The lower voltage decreases the sputter yield due to the lower incident energy.

Alternate processes have been investigated because the use of reactive DC magnetron sputtering has not been optimized for the deposition of such films. Pulsed DC power reactive magnetron sputtering seems to be one of the most promising processes [1,5,9,11,12]. Frequencies in the range of 10–200 kHz, applied to the target, can successfully eliminate arcing while sustaining relative high-metal deposition rates [1]. Also the control of partial reactive operating pressure, or flow rates [13] and arc suppression techniques [1] are beneficial in pulsed DC sputtering.

Besides the requirement of high deposition rates, the sputtered metal atoms are required to successfully fill high aspect ratio (AR) features (AR > 1) with insulating films in ultra-large scale integration (ULSI) technologies. The angular distribution of the sputtered atoms is roughly a cosine distribution, and is further broadened by gas phase scattering, yielding insufficient bottom coverage and voids during filling of high aspect ratio features. This problem is solved by ionizing the metal flux and applying a bias on the substrate, accelerating the metal ions through the plasma sheath near the substrate surface [14,15]. Since the sheath thickness is thinner than the mean free path and the electric field is normal to the substrate, a narrow angular distribution is achieved. Ionized physical vapor deposition (IPVD) is

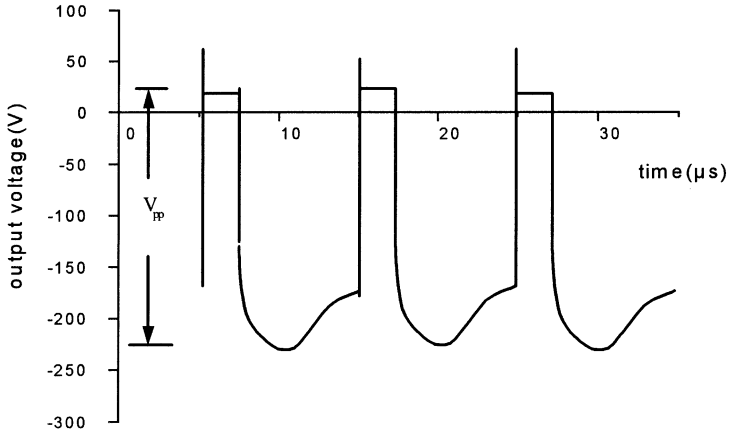

Fig. 2. Pulsed power wave form can effectively eliminate the arcs. Variation of the output affects the deposition process and film quality. Typical working points in this work: frequency = 100 kHz, pulse width = 20%, power = 2 kW, $V_{pp} \sim 250$ V.

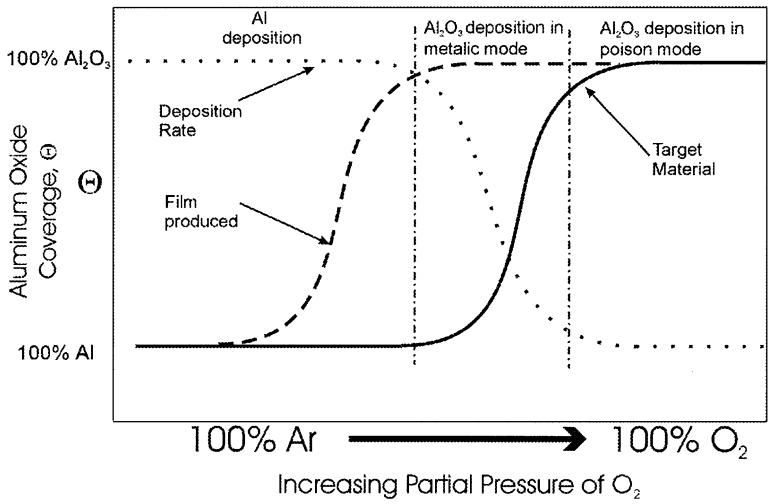

Fig. 3. Coverage of Al and Al_2O_3 at the substrate and on the target as a function of the partial pressure of O_2 gas in the chamber. As the O_2 component is extremely low, both the target and the substrate are mainly covered by pure Al, i.e. no Al_2O_3 is deposited on the substrate. Later, within a certain range of O_2 partial pressure, only the substrate is covered by Al_2O_3 while the target is still clean, This is called the metallic mode. And the deposition rate begins to drop. As the O_2 percentage exceeds some critical value, both the target and the substrate are covered by Al_2O_3, which is called poison mode. An abrupt drop of deposition rate occurs at this transition.

accomplished by adding an inductively coupled plasma (ICP) coil between the substrate and target [16–18]. Previous work has shown IPVD is advantageous over PVD both in high deposition rates as well as feature fillings in metal target sputtering [17,18]. It is also practical to use IPVD to make insulating films such as Al_2O_3 in combination with a pulsed power [19,20].

This paper investigates the benefit brought by IPVD in pulsed DC magnetron reactive sputtering of aluminum oxide films. Deposition rates are enhanced with the RF power at relative high total pressure. Electron density and electron temperature changes caused by the reactive gas partial pressure are measured by a Langmuir probe. SEM images of deposited films show differences in film morphology as a function of RF power. X-Ray photoelectron spectroscopy (XPS) characterizes the composition of the films.

2. Experiment

A commercial DC planar magnetron-sputtering tool is used along with a secondary-plasma to study IPVD processes and applications [17,18]. As in conventional PVD, a 33-cm diameter pure aluminum target (cathode) is mounted with a rotating magnet being able to process 200-mm wafers. The vacuum can be established to a base pressure of 6×10^{-5} Pa (4.5×10^{-7} torr) by a two-stage roughing pump and two CTI Cryogenic cryopumps. Ar and O_2 are introduced to the chamber as the sputtering gas and reactive gas, respectively. Both flow rates are controlled by MKS mass flow meters.

A seven-turn water-cooled helical resonator coil delivers a 13.56-MHz RF power to the plasma and generates a secondary inductively coupled plasma. This plasma can efficiently ionize the sputtered flux, achieving IPVD. The total length of the unwound aluminum, helical coil is equal to one-half of the wavelength of the RF. The mid-point of the coil can be grounded, but was not for this experiment. The coil is placed between the target and substrate with a diameter of 310 ± 20 mm. The matching network consists of three capacitors connected in parallel. The first is held constant at 600 pF, while the second and third capacitors can be varied between 0–600 pF and 0–150 pF, respectively. Adjusted to proper values, the capacitors work effectively to minimize the reflected RF power supply. The net RF power absorbed by the plasma is the subtraction of reflected power from the incident power $(500-24)$ W means 500 W forward and 24 W reflected. A cross-section of the chamber geometry, the seven-turn ICP coil and the diagnostic are shown in Fig. 1.

The aluminum target is powered by an ENI RPG-100 pulsed directed current DC power unit, which functions to generate the first sputtering plasma in the vicinity of the aluminum target. This unit discharges the accumulated ions on the insulating AlO_x film surface during the positive duty cycle and suppresses arc formation. The unit utilizes a maximum arc count function to shut down power output when this count is reached, typically approximately 1000 counts. Several parameters of the output waveform can be adjusted to minimize arcing, thus protecting the substrate and deposited film from small metal droplets. The tradeoff is that low pulsed-power frequency tends to increase deposition rate (more like DC), while a higher frequency improves plasma chemistry, enhancing film uniformity, resistivity and

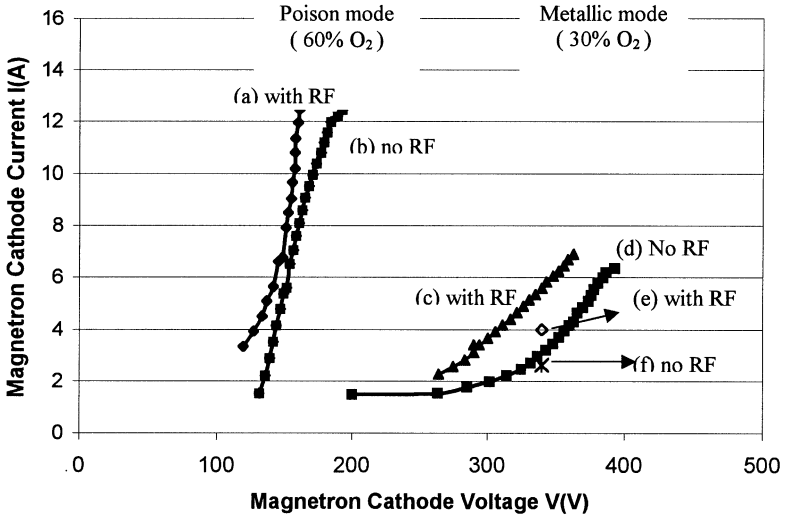

Fig. 4. Typical *I–V* traces of IPVD in the reactive sputtering at the total pressure of 3.33 Pa. Curves (a–d) demonstrate different conductivity of the plasma under different reactive sputtering modes. The two individual data, (e) and (f) were taken with Ar only.

AlO_x composition. The typical values chosen for pulsed power frequency and pulse width are 100 kHz and 2100 ns, respectively. The reverse voltage (positive) is approximately 10% of the negative voltage. In this experiment, the power is kept at 2 kW, the negative voltage is in the range of 200–250 V. Fig. 2 depicts the pulsed width configuration.

A water-cooled quartz crystal microbalance (QCM) and a three-layer-gridded energy analyzer (GEA) located in the plane of horizontal substrate surface are utilized to measure deposition rate and ionization fraction of the metal species. The top grid is grounded and the middle and bottom one are biased with the same voltage. The plasma has a positive potential with respect to the grounded top grid due to the formation of the plasma sheath, roughly in the order of 20 V. Since the mean free path in this experiment is far less than the distance between the substrate and target, oxygen negative ions formed and accelerated near the target cannot reach the substrate with enough energy to transit the plasma sheath. Therefore, negative ions cannot reach the QCM. When the bottom two grids are biased −30 V, both

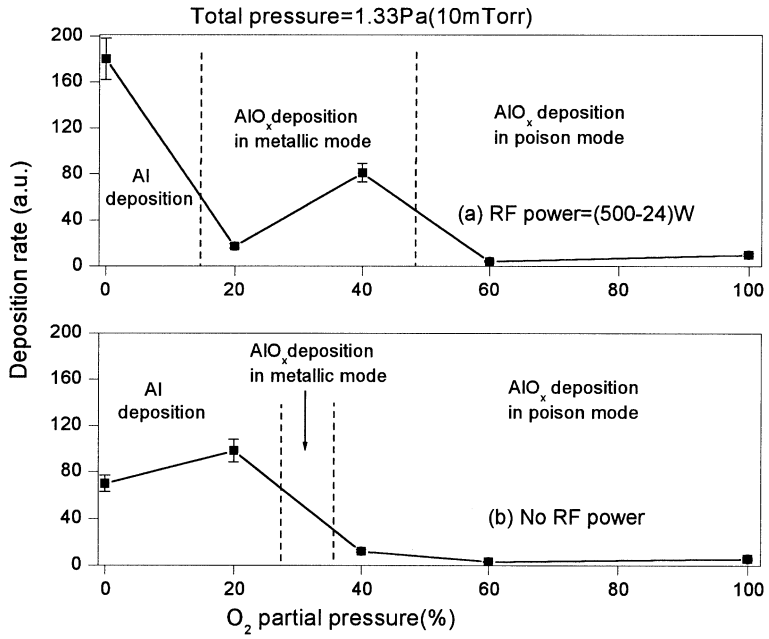

Fig. 5. Deposition rate variation with O_2 partial pressure change under total pressure of 1.33 Pa. The process is divided into three regions according to the variation. The error bars for the deposition measurements are approximately ±10%.

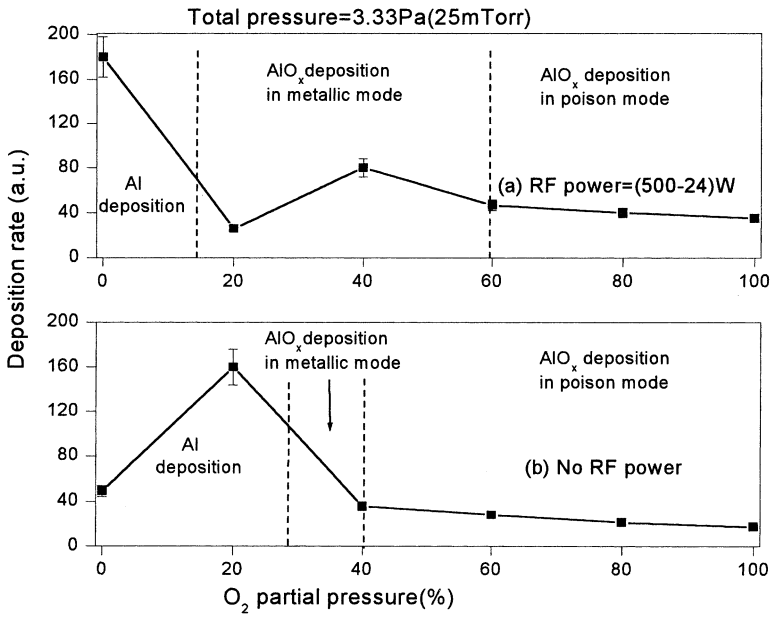

Fig. 6. Deposition rate vs. O_2 partial pressure change under total pressure of 3.33 Pa. The error bar for the deposition measurement is approximately $\pm 10\%$.

aluminum positive ions and neutral atoms diffuse to the crystal sensor and deposit on it. The deposition rate of the two species, $D_{\text{ions}}+D_{\text{neutrals}}$, can be determined by an XTC/2 deposition controller. While the bottom two grids are biased +30 V, positive ions are repelled and only neutral aluminum species deposit, thus obtaining D_{neutrals}. Therefore, the ionization fraction is calculated by the two sets of data:

$$\text{Ionization fraction}=\frac{D_{\text{ion}}}{D_{\text{ion}}+D_{\text{neutral}}} \quad (1)$$

Deposition rates are taken at the throw distance of 15 cm and are calibrated with film thickness profilometer measurements on a silicon substrate. Calibration of the measured data accounts for the transparency of the grids, chamber geometry, and scattering. Calibration was done for a pure Al deposition and for an AlO_x deposition at 40% oxygen partial pressure. This procedure is explained in detail in earlier papers [17]. Film thickness is measured based on the following formula [21]:

$$T_{\text{f}}=\left(\frac{N_{\text{at}}d_{\text{q}}}{\pi d_{\text{f}}F_{\text{c}}Z}\right)\arctan\left(Z\tan\left(\frac{\pi(F_{\text{q}}-F_{\text{c}})}{F_{\text{q}}}\right)\right) \quad (2)$$

where Z represents Z-ratio and is a function of film density and shear modulus and T_{f}, film thickness; N_{at}, frequency constant of AT cut quartz = 166 100 Hz cm; d_{q}, density of single crystal quartz = 2.649 g/cm^3; d_{f}, film density; F_{q}, quartz crystal with uncoating frequency; and F_{c}, quartz crystal with coating frequency.

For a quartz crystal frequency change of 2% F_{q}, the Al film thickness change is 1.456 times that of an Al_2O_3 film. Therefore, different calibrations are used if the film is believed to be Al or Al_2O_3 since their density and Z-ratios differ. If the film was conductive, the Al values were used. If the film was an insulator, the Al_2O_3 values were used. The density and Z-ratio of AlO_x with various x values are unknown. We believe the error introduced by this procedure falls within the reported error bars.

A Hitachi S4700 is used for SEM images to assess film morphology. XPS was used to determine the composition of AlO_x at the 40% O_2 (RF on) point, where x was found to be 1.75, a bit more O rich than the ideal ratio of 1.5 for Al_2O_3, without presputtering.

3. Results

There are two modes of operation for reactive sputtering that should be considered in depositing a compound film. Fig. 3 is a qualitative graph which explains how the film produced and the target material change as a function of increasing O_2 partial pressure. Two deposition conditions for Al_2O_3 are apparent: 'metallic' mode, where the target is still pure metal, and 'poison' mode where the target has become covered with Al_2O_3. Note that in general, as depicted in Fig. 3, higher deposition rates are achieved in the 'metallic mode' than in 'poison mode'. For fixed total pressure, as the reactive gas flux is varied, there is a transition between the poison and metallic modes which can exhibit hysterisis.

The addition of an inductively-coupled (ICP) coil to generate a secondary plasma produces more Ar ions, more Al ions and more O radicals, which changes the transition point between the modes and the variation of

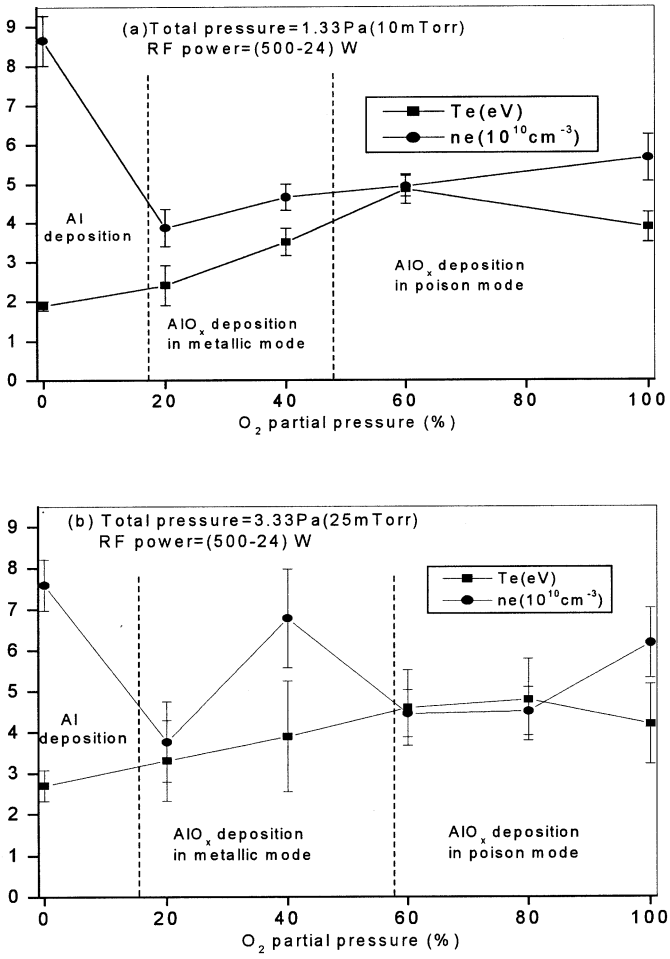

Fig. 7. Electron temperature and electron density change with the O_2 partial pressure with total pressure of 1.33 Pa and 3.33 Pa. These are the two main factors affecting the ionization fraction of the Al atom.

deposition rate with the O_2 partial pressure. With the RF power on, the metallic mode occurs at a wider range of reactive gas partial pressure than without the RF power. Since the number of Al ions also increases with the addition of RF, the deposition rate goes up as the RF power is applied.

Depending on the working condition, the impedance of the target–plasma–ground circuit differed as shown in the current–voltage (I–V) traces (Fig. 4). A higher magnetron cathode current was induced at a given voltage when the RF power to the ICP coil is on, regardless of whether one is in metallic or poison mode, due to increased ionization of both aluminum atoms and gas atoms caused by the secondary plasma. Since a higher ion-induced secondary electron emission rate exists for aluminum oxide compared to pure aluminum [10], magnetron cathode current increases with any coverage of aluminum oxide ($\Theta > 0$) on the target. Therefore, the behavior in metallic mode vs. poison mode is quite distinct.

In addition to the four curves shown in Fig. 4, two data points (shown in Fig. 4) were taken with Ar only. Note that a higher current was still obtained with the RF on, though not as high as when O_2 was present. The even higher current with O_2 present is due to RF power producing O radicals which can oxidize the target away from the sputtering track and therefore raises the secondary electron component of the current. Once the target was heavily covered with aluminum oxide (far into poison mode, 100% O_2), the secondary electrons dominated the current, and the addition of RF power did not change the current significantly.

Deposition rates were measured under different O_2 partial pressures and total ($Ar+O_2$) pressures. These rates are presented in Figs. 5 and 6. Fig. 5a,b are the deposition rates vs. oxygen partial pressure at 1.33 Pa (10 mtorr) total pressure, with the RF power on and off, respectively. Each figure is divided into three regions as explained in the figure. The placement of the dashed lines is approximate and could vary $\pm 5\%$. Several

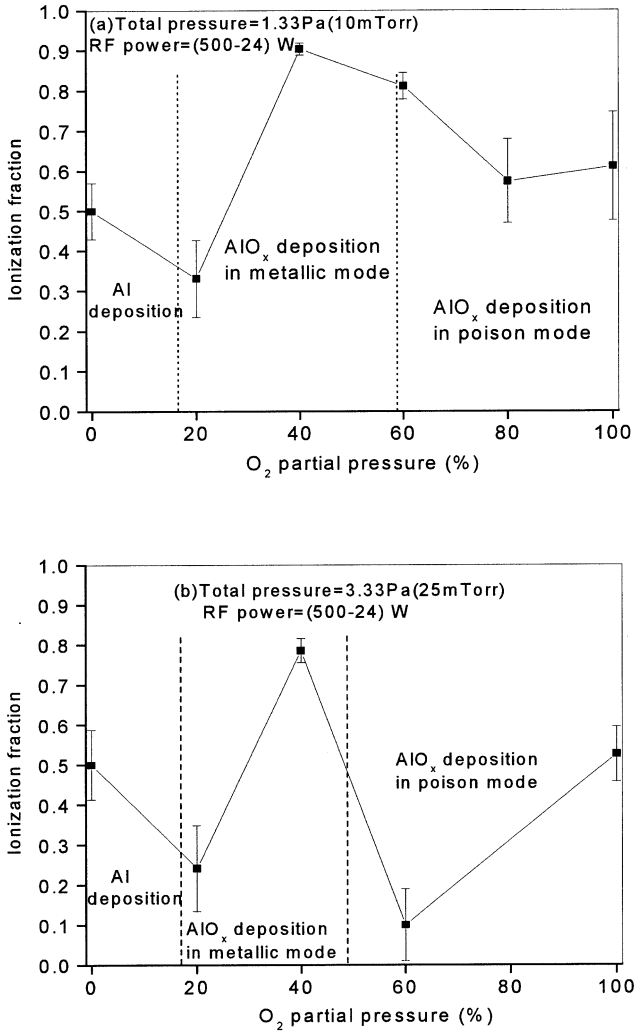

Fig. 8. Ionization fraction changes with the O_2 partial pressure at the incident RF power of 500 W.

combined factors determine the variation of deposition rates with the reactive partial pressure: the number of aluminum atoms sputtered from the target, the aluminum oxide coverage on the target, the electron temperature, and electron density of the ICP plasma.

In the first region of Fig. 5a, the O_2 partial pressure was still low (less than 20%), both the target and substrate were covered mainly by pure aluminum, and only aluminum was deposited on the substrate (as described in Fig. 3). Total pressure was fixed, so as the argon density is decreased, the O_2 partial pressure increases, resulting in a lower sputtering rate of the aluminum target and a dramatic drop in the deposition rate. The sputtering rate drops because even some oxygen coverage of the surface effectively increases the surface binding energy of aluminum atoms. This effect is exacerbated due to preferential sputtering of Al over Al_2O_3 and decreases the yield [22] further. Comparing the first point in Fig. 5a to the first point in Fig. 5b, when the RF is on, More sputtering occurs due to more Ar^+. In addition, aluminum atoms are ionized by the secondary plasma and deposited directionally to the substrate. Therefore for a pure aluminum target, the deposition rate with a secondary plasma is greater than without a secondary plasma.

The second region contains a higher percentage of O_2 partial pressure, where aluminum oxide began to deposit on the substrate while the target was mostly clean (metallic mode). In this region the electron temperature (Fig. 7a) increased as more O_2 was present dramatically increasing the ionization fraction (Fig. 8a). In addition, the O^+ also contributes to the sputtering process. According to transport of ions in matter (TRIM) [23] simulation of sputtering to an Al_2O_3 layer with the thickness of 1000 Å, the sputter yield of aluminum by O^+ bombardment is much larger than by Ar^+ bombardment. For example, for a 300-eV normal incidence, the aluminum sputtering yield due to O^+ bombardment of Al_2O_3 is 0.968 compared to 0.422 due to argon bombardment. Consequently more energy is transferred to target atoms from oxygen bombardment than from argon bombardment, and sputtering of aluminum as well as aluminum from Al_2O_3, is more efficient. As the Al_2O_3 coverage grows the effect of ionization and O^+ sputtering on deposition rate reaches a maximum and preferential sputtering effects take over. It is more likely to sputter O than Al from fully covered Al_2O_3 targets. At that point the Al deposition curve begins to decrease. Fig. 5a shows the maximum value happened at O_2 partial pressure of approximately 40% and reached nearly half of the aluminum deposition rate in pure Ar.

In the poison mode region, the third region of Fig. 5a, both the target and substrate were covered by AlO_x and few Al atoms were sputtered. Formation of oxides on the target leads to a substantial decrease in aluminum sputtering due to preferential sputtering of the oxygen as well as an effective increase of the surface binding energy of the target atoms [10]. These factors explain the substantial drop of deposition rate, as low as one-tenth of aluminum deposition rate in pure Ar.

Fig. 5b is the deposition rate variation with partial pressure of O_2 at a total pressure of 1.33 Pa (10 mtorr) while the RF power was off. Compared to Fig. 5a the variation was simple and was only affected by the AlO_x coverage of the target. The deposition rates were lower than the Fig. 5a case when AlO_x was deposited. Also, the RF power extended the region of O_2 partial pressure in the desirable metallic mode deposition of AlO_x as shown in Fig. 5a. This is because (1) the RF power generated more Ar^+ ions, which are accelerated by the cathode voltage to sputter the target surface and slow down the formation of AlO_x on the target surface,

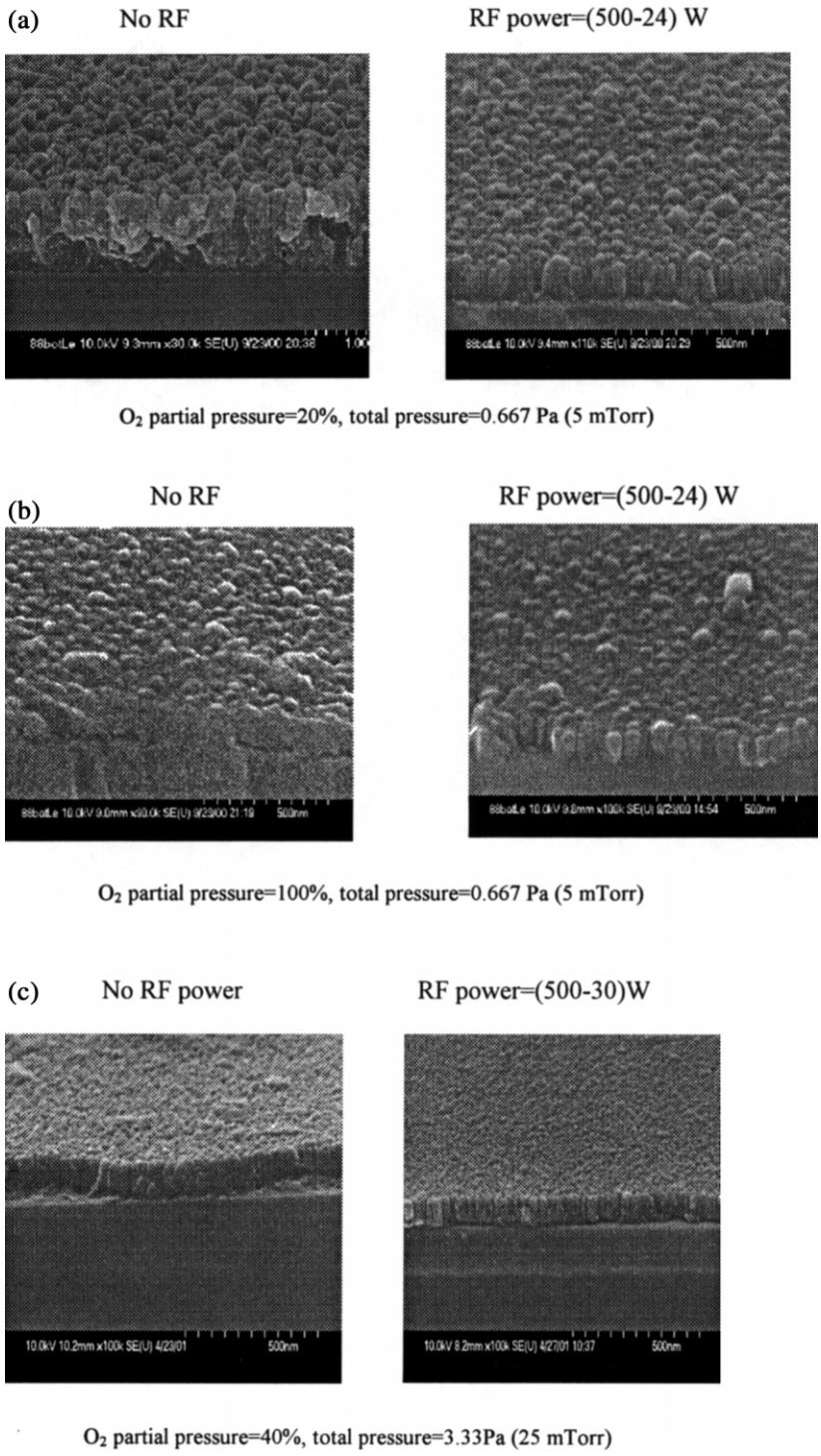

Fig. 9. Comparison of SEM pictures between RF power on and RF power off, at different O_2 partial pressures and different total pressure ($Ar+O_2$).

even though more O radicals are now present; and (2) the substrate does not undergo any sputtering due to the low sheath voltage and this permits more oxidation of the deposited film. In turn, with lower AlO_x target coverage, oxygen sputtering dominates and more aluminum is sputtered as explained earlier. The fact that RF power dissociates more O_2 molecules into O atoms, which are consequently responsible for the formation of aluminum oxide is most apparent at the substrate where no sputtering occurs. That is why aluminum oxide

deposition is obtained at lower O_2 partial pressure, with a secondary plasma present.

Fig. 6a,b are the deposition rates vs. oxygen partial pressure at 3.33 Pa (25 mtorr) total pressure with the RF power on, while Fig. 6b is the same condition with the RF power off. Fig. 6a shows deposition rate variation with oxygen partial pressure at a total pressure of 3.33 Pa (25 mtorr) with the RF power on. The variation is similar to that of Fig. 5 — except that the metallic mode region is wider. With the RF on, the mechanisms involved are the same as in the 1.33-Pa (10-mtorr) case. With the absence of a secondary plasma (RF off), O^+ sputtering dominates in the first region since at a higher pressure, a greater number of O^+ will exist. Thus, an increase in deposition rate is seen in Fig. 6b. However, since more of these oxygen ions will react with the target, the deposition rate will reach a maximum and based on preferential sputtering, the deposition rate will begin to decrease.

Ionization fraction of the Al atoms at 3.33 Pa (25 mtorr) total pressure was higher than that of 1.33 Pa (10 mtorr), as Fig. 8 shows. The ionization fractions go to a maximum value of 90% (3.33 Pa) ionization fraction in metallic mode due to the increase of electron temperature (see Fig. 7). The electron temperature did not vary significantly beyond that point, but the ionization fractions dropped because the electron density reached a minimum approximately 80% O_2 partial pressure. The presence of O^- ions likely decreased the density of electrons at the highest O_2 partial pressures. At 100% O_2 partial pressure, there was a rise in ionization fraction at both 1.33 and 3.33 Pa due possibly to the dynamics of the electronegative gas.

Fig. 9 shows SEM images of film formed on the silicon substrates. Fig. 9a is for the cases of 20% O_2 partial, and Fig. 9b is for 100% O_2 partial pressure. Both cases included data with and without RF power at a total pressure of 0.667 Pa (5 mtorr). At 0.667 Pa (5 mtorr) total pressure, with 20% O_2, (Fig. 9a) the deposited film was AlO_x when RF was present, while pure aluminum film was only obtained when the RF was absent. As discussed in the deposition rate figure, RF power shifts the onset of metallic mode AlO_x deposition. When RF is on, the secondary ionization increased positive ion bombardment to the film, thus densifying it. Without RF power, the film shows porous columnar structure. In the 100% O_2 case SEM images shown in Fig. 9b, the film made without the RF looks like molten droplets; but the RF power and subsequent ion bombardment keeps the column structure, and film is smoother. Fig. 9c shows the morphology of films made at 3.33 Pa (25 mtorr) total pressure with 40% O_2, both with a heated substrate of 220°C. The ion bombardment produced by the RF power makes the film denser and smoother, and the grain structure is finer and more complete.

4. Conclusions

IPVD is advantageous over conventional PVD in reactive sputtering for three reasons. First, the ICP extends the metallic mode operating range of reactive sputtering of AlO_x. Ionization fraction and deposition rate can be maximized by controlling the reactive gas partial pressure. This variation of deposition rate and ionization fraction with the reactive gas partial pressure was due to the combined reasons of target coverage, number of Al atoms sputtered off, electron temperature and electron density of the inductively coupled plasma. Second, the deposition rate of AlO_x was higher with the RF power on than without. Lastly, the increased ionization fraction contributes to ion bombardment of the film on the substrate and creates a denser and smoother film.

Acknowledgements

NSF/DOE Basic Plasma Science Initiative, DE-FG02-97ER54440 supplies part of the funding and MRC (Now TEL, Arizona) donated the commercial magnetron. CVC Corp. (now Veeco & CVC) partially funded the work and donated the RPG-100 pulsed power supply. SEM work was carried out in the Center for Microanalysis of Materials, University of Illinois, which is partially supported by the US Department of Energy under grant DEFG02-96-ER45439. Vania Petrova is acknowledged for assistance in SEM work.

References

[1] P.J. Kelly, J. Vac. Sci. Technol. A 17 (3) (1999) 945.
[2] J. Kolodzey, Appl. Phys. Lett. 71 (26) (1997) 3802.
[3] C. Deshpandey, L. Holland, Thin Solid Films 96 (1982) 265.
[4] M. Scherer, J. Schmitt, R. Latz, M. Schanz, J. Vac. Sci. Technol. A 10 (1992) 1772.
[5] P. Frach, U. Heisig, Chr. Gottfried, H. Walde, Surf. Coat. Technol. 59 (1993) 177.
[6] K.K. Shih, D.B. Dove, J. Vac. Sci. Technol. A 12 (1994) 321.
[7] B. Lux, C. Colombier, H. Altena, K. Stjemberg, Thin Solid Films 138 (1986) 49.
[8] D.A. Glocker, J. Vac. Sci. Technol. A 11 (1993) 2829.
[9] W.D. Sproul, M.E. Graham, M.S. Wong, S. Lopez, D. Li, R.A. Scholl, J. Vac. Sci. Technol. A 13 (1995) 1188.
[10] W.D. Westwood, in: S.M. Rossnagel, J.J. Cuomo, W.D. Westwood (Eds.), Handbook of Plasma Processing, Noyes Publications, Park Ridge, New Jersey, USA, 1990, pp. 233–257.
[11] A. Belkind, A. Freilich, J. Vac. Sci. Technol. A 17 (4) (1999) 1934.
[12] J.M. Schneider, W.D. Sproul, R.W.J. Chia, M.-S. Wong, A. Matthews, Surf. Coat Technol. 96 (1997) 262–266.
[13] M. Kharrazi Olson, J. Vac. Sci. Technol. A 16 (2) (1998) 639.
[14] P.F. Cheng, S.M. Rossnagel, D.N. Ruzic, J. Vac. Sci. Techol. B 13 (2) (1995) 203–208.

[15] S.M. Rossnagel, J. Hopwood, Appl. Phys. Lett. 63 (1993) 24.
[16] S.M. Rossnagel, Thin Solid Films 263 (1995) 1.
[17] M.M.C. Allain, D.B. Hayden, D.R. Juliano, D.N. Ruzic, J. Vac. Sci. Technol. A 18 (3) (2000) 797.
[18] D.B. Hayden, D.R. Juliano, M.N. Neumann, M.C. Allain, D.N. Ruzic, Surf. Coat. Technol. 120\121 (1999) 401–404.
[19] J.M. Schneider, W.D. Sproul, A.A. Voevodin, A. Matthews, J. Vac. Sci. Technol. A 15 (1997) 1084–1088.
[20] J.M. Schneider, W.D. Sproul, A. Matthews, Surf. Coat. Technol. 98 (1998) 1473–1476.
[21] Leybold XTC/C XTC/s User Guide, 5–11, part number 074-183/041795.
[22] R. Kelly, N.Q. Lam, Rad. Effects 19 (1) (1973) 39.
[23] J.P. Biersack, W. Eckstein, Appl. Phys. A 34 (1984) 73.